Journal of Solid Mechanics Vol. 8, No. 3 (2016) pp. 466-481

Thermoelastic Analysis of Rotating Thick Truncated Conical Shells Subjected to Non-Uniform Pressure

M. Jabbari [1], M. Zamani Nejad [1,*], M. Ghannad [2]

[1]*Mechanical Engineering Department, Yasouj University, Yasouj, Iran*
[2]*Mechanical Engineering Faculty, Shahrood University, Shahrood, Iran*

Received 28 March 2016; accepted 23 May 2016

ABSTRACT

In the present work, a study of thermoelastic analysis of a rotating thick truncated conical shell subjected to the temperature gradient and non-uniform internal pressure is carried out. The formulation is based on first-order shear deformation theory (FSDT), which accounts for the transverse shear. The governing equations, derived using minimum total potential energy principle, are solved, using multi-layered method (MLM). The model has been verified with the results of finite element method (FEM) for several tapering angles of the truncated cone. The numerical results obtained are presented graphically and the effects of thermal and mechanical loading, tapering angle of truncated cone, and profile of internal pressure are studied in detail.

Keywords : Truncated conical shells; Thick shells; Thermoelastic analysis; Rotation; Non-uniform pressure.

1 INTRODUCTION

ROTATING conical shells are increasingly being put to numerous engineering applications such as hoppers, vessel heads, components of missiles and spacecrafts, heart ventricles, diffusers and other civil, mechanical and aerospace engineering structures [1]. Since in most applications, conical shells must operate under extremes of thermal and mechanical loadings, any failure or fracture will be an irreparable disaster. So, adequate strength consideration is so important for these components [2].

From early thermoelastic analyses on conical shells, Witt [3] derived a differential equation of a conical shell subjected to axis-symmetrical temperature distributions. In order to obtain a particular solution to the differential equation, he assumed the expression for the temperature distributions to be the sum of hyperbolic and cubic functions. Panferov [4] used the method of successive approximations to obtain the solution of the problem of thermal loading of an elastic truncated conical pipe with constant thickness. A generalized thermoelasticity problem of multilayered conical shells was presented in Jane and Wu [5]. They developed a hybrid Laplace transformation and finite difference to obtain the solution of two-dimensional axisymmetric coupled thermo-elastic equations. Patel et al. [6] studied the thermoelastic post-buckling behavior of cross-ply laminated composite conical shells under presumed uniform temperature distribution. Vivio and Vullo [7] presented an analytical procedure for the evaluation of elastic stresses and strains in rotating conical disks, either solid or annular, subjected to thermal load, with a fictitious density variation along the radius.

Naj et al. [8] studied thermal and mechanical instability of truncated conical shells made of functionally graded materials. Based on the perturbation theory, Eipakchi et al. [1,9] used a mathematical approach for axisymmetric

*Corresponding author. Tel.: +98 74 33221711; Fax: +98 74 33221711.
E-mail address: m_zamani@yu.ac.ir (M. Zamani Nejad).

stress analysis of a thick conical shell with varying thickness under nonuniform internal pressure. By applying a meshless local Petrov-Galerkin method, Saldek et al. [10] solved problems of Reissner-Mindlin shells under thermal loading. Using the tensor analysis, Nejad et al. [11] obtained a complete and consistent 3D set of field equations to characterize the behavior of functionally graded (FG) thick shells of revolution with arbitrary curvature and variable thickness. Ghannad et al. [12] obtained an elastic solution for thick truncated conical shells. They employed the FSDT for the analysis of the problem. Arefi and Rahimi [13] investigated thermoelastic analysis of a functionally graded cylinder under mechanical and thermal loads. Jabbari et al. [14] presented the general solution of steady-state two-dimensional non-axisymmetric mechanical and thermal stresses and mechanical displacements of a hollow thick cylinder made of fluid-saturated functionally graded porous material.

More recently, Ray et al. [15] carried out an analysis of conduction heat transfer through conical shells of different inner radii and shell thicknesses. Based on the high-order shear deformation theory (HSDT), Ghannad and Gharooni [16] presented displacements and stresses for axisymmetric thick-walled cylinders made of functionally graded materials under internal and/or external uniform pressure by using the infinitesimal theory of elasticity and analytical formulation. Ghannad et al. [17] performed an elastic analysis for axisymmetric clamped-clamped pressurized thick truncated conical shells made of functionally graded materials. In other work, using matched asymptotic method of the perturbation theory, Ghannad et al. [18] presented an analytical solution for deformations stresses of axisymmetric clamped–clamped thick cylindrical shells with variable thickness made of functionally graded materials subjected to internal pressure.

Nejad et al. [19] used a semi-analytical iterative method as one of the newest analytical methods for the elastic analysis of thick-walled spherical pressure vessels made of functionally graded materials subjected to internal pressure. Nejad et al. [20] derived an elastic solution for the purpose of determining displacements and stresses in a thick truncated conical shell under uniform pressure where MLM has been used for solution. They also used this method to the analysis of a rotating truncated conical shell [21]. Making use of FSDT and MLM, Nejad et al. [22] performed a semi-analytical solution for the purpose of elastic analysis of rotating thick truncated conical shells made of functionally graded material (FGM) under non-uniform pressure.

In this paper, thermo-elastic analysis of rotating thick truncated conical shells under non-uniform pressure is considered. The governing equations are based on FSDT that accounts for the transverse shear. The governing equations are derived, using minimum total potential energy principle. The heat conduction is also taken into consideration in the analysis. These equations in the axisymmetric case and thermo-elasto-static state constitute a system of ordinary differential equations with variable coefficients. Normally, these equations do not have exact solutions. The MLM is used to solve the system of equations with variable coefficients. For this purpose, a rotating truncated conical shell is divided into disks with constant thickness. With regard to the continuity between layers and applying boundary conditions, the governing set of differential equations with constant coefficients is solved. In fact, this technique converts the set of equations with variable coefficient into the set of equations with constant coefficient. The results are compared with those derived through the finite element method (FEM) for some load cases. By numerically solving the resulting equations, the distribution of the thermal stress and displacement components can be obtained and the numerical results of the thermal stresses are presented graphically to show the effect of loading parameters on the distribution of thermal stresses and displacements. In particular, we studied the influence of tapering angles on the results. Finally, the conclusions drawn from the present study are reported.

2 GOVERNING EQUATION

In the FSDT, the sections that are straight and perpendicular to the mid-plane remain straight but not necessarily perpendicular after deformation and loading. In this case, shear strain and shear stress are taken into consideration. The geometry of a thick truncated cone with thickness h, and the length L, is shown in Fig. 1. The location of a typical point m, within the shell element is

$$\begin{cases} m:(r,x)=(R+z,x) \\ 0\le x\le L \quad \& \quad -\dfrac{h}{2}\le z\le \dfrac{h}{2} \end{cases} \tag{1}$$

where z is the distance of a typical point from the middle surface. In Eq. (1), R represents the distance of the middle surface from the axial direction.

$$R(x) = a + \frac{h}{2} - (\tan\beta)x \tag{2}$$

where β is half of tapering angle as:

$$\beta = \tan^{-1}\left(\frac{a-b}{L}\right) \tag{3}$$

For axial distribution of inner pressure P, the model of Eq. (4) is selected:

$$P = P_1 + (P_2 - P_1)\left(\frac{x}{L}\right)^m \tag{4}$$

Here P_1 and P_2 are the values of pressure at the $x = 0$ and $x = L$, respectively and m is a constant parameter, which is used to control the pressure profile. The pressure applied to the internal surface is comprised of two components as follows

$$P_x = P\sin\beta \quad , \quad P_z = P\cos\beta \tag{5}$$

where P_x and P_z are components of internal pressure P along axial and radial directions, respectively.

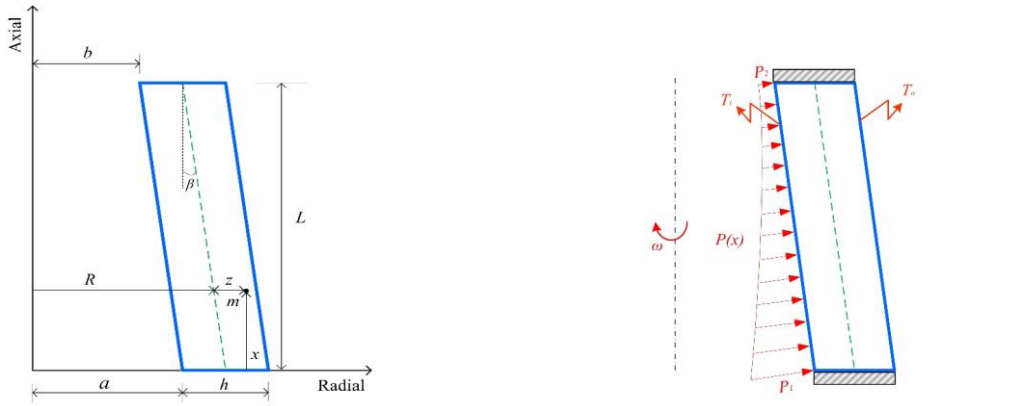

(a) Geometry parameters (b) Boundary and loading conditions

Fig.1
Cross section of the thick rotating truncated cone with clamped-clamped ends.

The general axisymmetric displacement field (U_x, U_z), in the FSDT could be expressed on the basis of axial displacement and radial displacement, as follows

$$U(x,z) = \begin{Bmatrix} U_x \\ U_z \end{Bmatrix} = \begin{Bmatrix} u(x) \\ w(x) \end{Bmatrix} + z \begin{Bmatrix} \phi(x) \\ \psi(x) \end{Bmatrix} \tag{6}$$

where $u(x)$ and $w(x)$ are the displacement components of the middle surface. In addition, $\phi(x)$ and $\psi(x)$ are the functions used to determine the displacement field. The kinematic equations (i.e., strain-displacement relations) in the cylindrical coordinates system are

$$\begin{cases} \varepsilon_x = \dfrac{\partial U_x}{\partial x} = \dfrac{du}{dx} + \dfrac{d\phi}{dx} z \\ \varepsilon_\theta = \dfrac{U_z}{r} = \left(\dfrac{w}{R+z} \right) + \left(\dfrac{\psi}{R+z} \right) z \\ \varepsilon_z = \dfrac{\partial U_z}{\partial z} = \psi \\ \gamma_{xz} = \dfrac{\partial U_x}{\partial z} + \dfrac{\partial U_z}{\partial x} = \left(\phi + \dfrac{dw}{dx} \right) + \dfrac{d\psi}{dx} z \end{cases} \tag{7}$$

Considering the effect of the thermal strain for homogeneous and isotropic materials, the stress-strain relations (i.e., constitutive equations) are as follows

$$\begin{cases} \begin{Bmatrix} \sigma_x \\ \sigma_\theta \\ \sigma_z \end{Bmatrix} = \lambda \begin{bmatrix} 1-\nu & \nu & \nu \\ \nu & 1-\nu & \nu \\ \nu & \nu & 1-\nu \end{bmatrix} \begin{Bmatrix} \varepsilon_x \\ \varepsilon_\theta \\ \varepsilon_z \end{Bmatrix} - \lambda\alpha(1+\nu)T \\ \tau_{xz} = \dfrac{E}{2(1+\nu)} \gamma_{xz} \end{cases} \tag{8}$$

where σ_i and $\varepsilon_i, i = x, \theta, z$ are the stresses and strains in the axial, circumferential, and radial directions. ν, E, α and T are Poisson's ratio, modulus of elasticity, the coefficient of thermal expansion and temperature gradient, respectively. In Eq. (8), λ is

$$\lambda = \frac{E}{(1+\nu)(1-2\nu)} \tag{9}$$

The normal forces (N_x, N_θ, N_z), bending moments (M_x, M_θ, M_z), shear force (Q_x), and the torsional moment (M_{xz}) in terms of stress resultants are

$$\begin{Bmatrix} N_x \\ N_\theta \\ N_z \end{Bmatrix} = \int_{-h/2}^{h/2} \begin{Bmatrix} \sigma_x \left(1 + \dfrac{z}{R}\right) \\ \sigma_\theta \\ \sigma_z \left(1 + \dfrac{z}{R}\right) \end{Bmatrix} dz \tag{10}$$

$$\begin{Bmatrix} M_x \\ M_\theta \\ M_z \end{Bmatrix} = \int_{-h/2}^{h/2} \begin{Bmatrix} \sigma_x \left(1 + \dfrac{z}{R}\right) \\ \sigma_\theta \\ \sigma_z \left(1 + \dfrac{z}{R}\right) \end{Bmatrix} z dz \tag{11}$$

$$Q_x = K \int_{-h/2}^{h/2} \tau_{xz} \left(1 + \frac{z}{R}\right) dz \tag{12}$$

$$M_{xz} = K \int_{-h/2}^{h/2} \tau_{xz} \left(1 + \frac{z}{R}\right) z dz \tag{13}$$

where K is the shear correction factor that is embedded into the shear stress term. In the static state, for conical shells $K = 5/6$ [23]. On the basis of the principle of virtual work, the variations of strain energy are equal to the variations of work of external forces as follows

$$\delta U = \delta W \tag{14}$$

where U is the total strain energy of the elastic body and W is the total work of external forces due to internal pressure and centrifugal force. With substituting strain energy and work of external forces, we have

$$\begin{aligned}&\int_0^L R \int_{-h/2}^{h/2} \left(\sigma_x \delta\varepsilon_x + \sigma_\theta \delta\varepsilon_\theta + \sigma_z \delta\varepsilon_z + \tau_{xz}\delta\gamma_{xz}\right)\left(1+\frac{z}{R}\right)dzdx = \int_0^L \left(P_x \delta U_x + P_z \delta U_z\right)\left(R-\frac{h}{2}\right)dx \\ &-\rho\omega^2 \int_0^L \int_{-h/2}^{h/2} \left(R+z\right)^2 \delta U_z dzdx\end{aligned} \tag{15}$$

Here ρ stands for the mass density, ω represents the constant angular velocity and $\rho\omega^2$ is the force per unit volume due to centrifugal force. Substituting Eqs. (7) and (8) into Eq. (15), and drawing upon the calculus of variation and the virtual work principle, we will have

$$\begin{cases} N_x R = C_0 - \int P_x \left(R-\dfrac{h}{2}\right)dx \\ M_x \dfrac{dR}{dx} + R\left(\dfrac{dM_x}{dx} - Q_x\right) = P_x \dfrac{h}{2}\left(R-\dfrac{h}{2}\right) \\ Q_x \dfrac{dR}{dx} + R\left(\dfrac{dQ_x}{dx}\right) - N_\theta = -P_z\left(R-\dfrac{h}{2}\right) - \dfrac{\rho\omega^2}{6}\dfrac{h}{2}\left(12R^2+h^2\right) \\ M_{xz}\dfrac{dR}{dx} + R\left(\dfrac{dM_{xz}}{dx} - N_z\right) - M_\theta = P_z \dfrac{h}{2}\left(R-\dfrac{h}{2}\right) - \dfrac{\rho\omega^2}{6}Rh^3 \end{cases} \tag{16}$$

and

$$\left[\left(N_x \delta u + M_x \delta\phi + Q_x \delta w + M_{xz}\delta\psi\right)R\right]_0^L = 0 \tag{17}$$

Eq. (17) states the boundary conditions which must exist at the two ends of the cone. In order to solve the set of differential Eqs. (16), with using Eqs. (7) and (13), and then using Eq. (16), we have

$$\begin{cases} \left[B_1\right]\dfrac{d^2}{dx^2}\{y\} + \left[B_2\right]\dfrac{d}{dx}\{y\} + \left[B_3\right]\{y\} = \{F\} \\ \{y\} = \{du/dx \quad \phi \quad w \quad \psi\}^T \end{cases} \tag{18}$$

The coefficients matrices $\left[B_i\right]_{4\times4}$, and force vector $\{F\}_{4\times1}$ are as follows

$$\left[B_1\right] = \begin{bmatrix} 0 & 0 & 0 & 0 \\ 0 & (1-\nu)\dfrac{h^3}{12}R & 0 & 0 \\ 0 & 0 & \mu h R & \dfrac{\mu h^3}{12} \\ 0 & 0 & \dfrac{\mu h^3}{12} & \dfrac{\mu h^3}{12}R \end{bmatrix} \tag{19}$$

$$[B_2]=\begin{bmatrix} 0 & (1-\nu)\frac{h^3}{12} & 0 & 0 \\ (1-\nu)\frac{h^3}{12} & (1-\nu)\frac{h^3}{12}\frac{dR}{dx} & -\mu hR & -(\mu-2\nu)\frac{h^3}{12} \\ 0 & \mu hR & \mu h\frac{dR}{dx} & 0 \\ 0 & (\mu-2\nu)\frac{h^3}{12} & 0 & \frac{\mu h^3}{12}\frac{dR}{dx} \end{bmatrix} \tag{20}$$

$$[B_3]=\begin{bmatrix} (1-\nu)hR & 0 & \nu h & \nu hR \\ 0 & -\mu hR & 0 & 0 \\ -\nu h & \mu h\frac{dR}{dx} & -(1-\nu)x & -h+(1-\nu)xR \\ -\nu hR & 0 & -h+(1-\nu)xR & -(1-\nu)xR^2 \end{bmatrix} \tag{21}$$

$$\{F\}=\frac{1}{\lambda}\begin{Bmatrix} C_0-\int P_x\left(R-\frac{h}{2}\right)dx+E\alpha(1+\nu)\int_{-h/2}^{h/2}(R+z)Tdz \\ P_x\frac{h}{2}\left(R-\frac{h}{2}\right) \\ -P_z\left(R-\frac{h}{2}\right)-\frac{\rho\omega^2}{6}\frac{h}{2}\left(12R^2+h^2\right)-E\alpha(1+\nu)\int_{-h/2}^{h/2}Tdz \\ P_z\frac{h}{2}\left(R-\frac{h}{2}\right)-\frac{\rho\omega^2}{6}Rh^3-E\alpha(1+\nu)\int_{-h/2}^{h/2}(R+2z)Tdz \end{Bmatrix} \tag{22}$$

where the parameters are as follows

$$\begin{cases} \mu=\frac{5}{12}(1-2\nu) \\ x=\ln\left(\frac{R+\frac{h}{2}}{R-\frac{h}{2}}\right) \end{cases} \tag{23}$$

3 SEMI-ANALYTICAL SOLUTION

3.1 Multi-layered formulation

In MLM, the truncated cone is divided into disk layers with constant thickness t, and constant height h(Fig. 2).

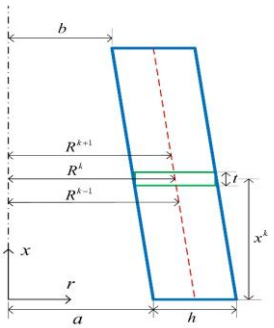

Fig.2
Dividing of truncated cone to disk form multilayer.

Therefore, the governing equations convert to nonhomogeneous set of differential equations with constant coefficients. $x^{[k]}$ and $R^{[k]}$ are represent length and radius of the middle of disks and k represents the number of disks. The modulus of elasticity and Poisson's ratio of disks assumed to be constant. The length of the middle of an arbitrary disk (Fig. 3) is as follows

$$\begin{cases} x^{[k]} = \left(k - \dfrac{1}{2}\right)\dfrac{L}{n} \\ \left(x^{[k]} - \dfrac{t}{2}\right) \le x \le \left(x^{[k]} + \dfrac{t}{2}\right) \\ t = \dfrac{L}{n} \end{cases} \tag{24}$$

where n is the number of disks and k is the corresponding number given to each disk. The radius of the middle point of each disk is as follows

$$R^{[k]} = a + \frac{h}{2} - \left(\tan\beta\right)x^{[k]} \tag{25}$$

Thus

$$\left(\frac{dR}{dx}\right)^{[k]} = \frac{dR^{[k]}}{dx^{[k]}} = -\tan\beta \tag{26}$$

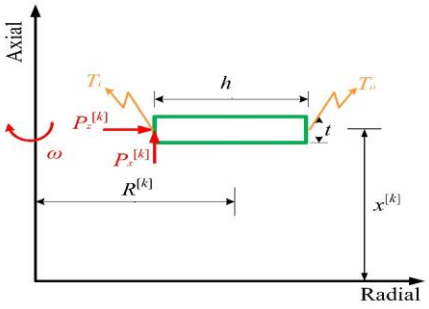

Fig.3
Geometry of an arbitrary disk layer.

3.2 Heat conduction equation

In the general form, the temperature distribution is the function of the axial and radial direction of the truncated cone. By dividing the truncated cone into disk form multilayer, the variation of temperature is assumed to occur in the radius direction only. By assumption of an element in the cylindrical coordinate system in the steady state without internal heat source, according to the heat balance equation for steady-state heat conduction without heat generation, the Eq. (27) for each disk has been conducted

$$\frac{d}{dr}\left(\kappa r \frac{dT}{dr}\right) = 0 \tag{27}$$

where k is the thermal conductivity coefficient. By considering Eq. (1) and Eq. (24), Eq. (27) can be written as follows

$$\frac{d}{dz}\left(\kappa\left(R^{[k]} + z\right)\frac{dT}{dz}\right) = 0 \tag{28}$$

Solving the differential Eq. (28) finally the terms of temperature gradient are derived as follows

$$T = d_1 \int_{-h/2}^{h/2} \frac{dz}{\kappa\left(R^{[k]}+z\right)} + d_2 - T_{ref} \tag{29}$$

where d_1 and d_2 are constants of integration and T_{ref} is the reference temperature. General boundary conditions for Eq. (29) are

$$\begin{cases} C_{11}T\big|_{z=-\frac{h}{2}} + C_{12}\left.\dfrac{dT}{dz}\right|_{z=-\frac{h}{2}} = f_1 \\ C_{21}T\big|_{z=\frac{h}{2}} + C_{22}\left.\dfrac{dT}{dz}\right|_{z=\frac{h}{2}} = f_2 \end{cases} \tag{30}$$

In Eq. (30), ($C_{ij}\, i=1,2; j=1,2$) are constants which depend on the thermal conductivity and the thermal convection. f_1 and f_2 are constants which are evaluated at the inner and outer radii, respectively. By exerting the boundary conditions for the temperature gradient distribution, we have

$$\begin{aligned} d_1 &= \frac{\left(C_{21}f_1 - C_{11}f_2\right)}{C_{11}C_{21}\ln\left(\dfrac{R^{[k]}+h/2}{R^{[k]}-h/2}\right) + \dfrac{C_{11}C_{22}}{R^{[k]}+h/2} - \dfrac{C_{21}C_{12}}{R^{[k]}-h/2}} \\ d_2 &= \frac{C_{21}\ln\left(R^{[k]}+h/2\right)f_1 - C_{11}\ln\left(R^{[k]}+h/2\right)f_2 + \dfrac{C_{22}f_1}{R^{[k]}+h/2} - \dfrac{C_{12}f_2}{R^{[k]}-h/2}}{C_{11}C_{21}\ln\left(\dfrac{R^{[k]}+h/2}{R^{[k]}-h/2}\right) + \dfrac{C_{11}C_{22}}{R^{[k]}+h/2} - \dfrac{C_{21}C_{12}}{R^{[k]}-h/2}} \end{aligned} \tag{31}$$

If the prescribed surface temperature imposed on inner and outer sides of each disk is

$$\begin{cases} C_{11}=1, C_{12}=0, f_1=T_i \\ C_{21}=1, C_{22}=0, f_2=T_o \end{cases} \tag{32}$$

If the $T_o = T_{ref}$, temperature gradient distribution is obtained as:

$$T^{[k]} = \left(T_o - T_i\right)\left(\frac{\ln\left(\dfrac{R^{[k]}+z}{R^{[k]}-h/2}\right)}{\ln\left(\dfrac{R^{[k]}+h/2}{R^{[k]}-h/2}\right)} - 1\right) \tag{33}$$

3.3 Thermoelastic solution

Considering shear stress and based on FSDT, the nonhomogeneous set of ordinary differential equations with constant coefficient of each disk is obtained.

$$\begin{cases} \left[B_1\right]^{[k]} \dfrac{d^2}{dx^2}\{y\}^{[k]} + \left[B_2\right]^{[k]} \dfrac{d}{dx}\{y\}^{[k]} + \left[B_3\right]^{[k]}\{y\}^{[k]} = \{F\}^{[k]} \\ \{y\}^{[k]} = \begin{Bmatrix} \left(\dfrac{du}{dx}\right)^{[k]} \\ \phi^{[k]} \\ w^{[k]} \\ \psi^{[k]} \end{Bmatrix} \end{cases} \tag{34}$$

The coefficients matrices $\left[B_i\right]_{4\times4}^{[k]}$, and force vector $\{F\}_{4\times1}^{k}$ are as follows

$$\left[B_1\right]^{[k]} = \begin{bmatrix} 0 & 0 & 0 & 0 \\ 0 & (1-\nu)\dfrac{h^3}{12}R^{[k]} & 0 & 0 \\ 0 & 0 & \mu h R^{[k]} & \dfrac{\mu h^3}{12} \\ 0 & 0 & \dfrac{\mu h^3}{12} & \dfrac{\mu h^3}{12}R^{[k]} \end{bmatrix} \tag{35}$$

$$\left[B_2\right]^{[k]} = \begin{bmatrix} 0 & (1-\nu)\dfrac{h^3}{12} & 0 & 0 \\ (1-\nu)\dfrac{h^3}{12} & -(1-\nu)\dfrac{h^3}{12}\tan\beta & -\mu h R^{[k]} & -(\mu-2\nu)\dfrac{h^3}{12} \\ 0 & \mu h R^{[k]} & -\mu h\tan\beta & 0 \\ 0 & (\mu-2\nu)\dfrac{h^3}{12} & 0 & -\dfrac{\mu h^3}{12}\tan\beta \end{bmatrix} \tag{36}$$

$$\left[B_3\right]^{[k]} = \begin{bmatrix} (1-\nu)hR^{[k]} & 0 & \nu h & \nu h R^{[k]} \\ 0 & -\mu h R^{[k]} & 0 & 0 \\ -\nu h & -\mu h\tan\beta & -(1-\nu)x^{[k]} & -h+(1-\nu)x^{[k]}R^{[k]} \\ -\nu h R^{[k]} & 0 & -h+(1-\nu)x^{[k]}R^{[k]} & -(1-\nu)x^{[k]}\left(R^{[k]}\right)^2 \end{bmatrix} \tag{37}$$

$$\{F\}^{[k]} = \frac{1}{\lambda}\begin{Bmatrix} C_0 - P\sin\beta\left(R^{[k]} - \dfrac{h}{2}\right)x + E\alpha(1+\nu)\displaystyle\int_{-h/2}^{h/2}\left(R^{[k]}+z\right)T^{[k]}dz \\ \dfrac{Ph}{2}\left(R^{[k]} - \dfrac{h}{2}\right)\sin\beta \\ -P\left(R^{[k]} - \dfrac{h}{2}\right)\cos\beta - \dfrac{\rho\omega^2}{6}\dfrac{h}{2}\left(12\left(R^{[k]}\right)^2 + h^2\right) + E\alpha(1+\nu)\displaystyle\int_{-h/2}^{h/2}T^{[k]}dz \\ \dfrac{Ph}{2}\left(R^{[k]} - \dfrac{h}{2}\right)\cos\beta - \dfrac{\rho\omega^2}{6}h^3R^{[k]} + E\alpha(1+\nu)\displaystyle\int_{-h/2}^{h/2}\left(R^{[k]}+2z\right)T^{[k]}dz \end{Bmatrix} \tag{38}$$

where the parameters are

$$\begin{cases} \mu = \dfrac{5}{12}(1-2\nu) \\ x^{[k]} = \ln\left(\dfrac{R^{[k]}+\dfrac{h}{2}}{R^{[k]}-\dfrac{h}{2}}\right) \end{cases} \tag{39}$$

Defining the differential operator $P(D)$, Eq. (27) is written as:

$$\begin{cases} \left[P(D)\right]^{[k]} = \left[B_1\right]^{[k]} D^2 + \left[B_2\right]^{[k]} D + \left[B_3\right]^{[k]} \\ D^2 = \dfrac{d^2}{dx^2} \quad , \quad D = \dfrac{d}{dx} \end{cases} \tag{40}$$

Thus

$$\left[P(D)\right]^{[k]} \{y\}^{[k]} = \{F\}^{[k]} \tag{41}$$

The above differential Equation has the total solution including general solution for the homogeneous case $\{y\}_h^{[k]}$ and particular solution $\{y\}_p^{[k]}$, as follows

$$\{y\}^{[k]} = \{y\}_h^{[k]} + \{y\}_p^{[k]} \tag{42}$$

For the general solution in the homogeneous case, $\{y\}_h^{[k]} = \{V\}^{[k]} e^{m^{[k]}x}$ is substituted in $\left[P(D)\right]^{[k]} \{y\}^{[k]} = 0$.

$$\left| m^2 \left[B_1\right]^{[k]} + m\left[B_2\right]^{[k]} + \left[B_3\right]^{[k]} \right| = 0 \tag{43}$$

The result of the determinant above is a six-order polynomial which is a function of *m*, the solution of which is a 6 eigenvalues m_i. The eigenvalues are 3 pairs of conjugated root. Substituting the calculated eigenvalues in the following equation, the corresponding eigenvectors $\{V\}_i$ are obtained.

$$\left[m^2 \left[B_1\right]^{[k]} + m\left[B_2\right]^{[k]} + \left[B_3\right]^{[k]} \right] \{V\}^{[k]} = 0 \tag{44}$$

Therefore, the homogeneous solution for is

$$\{y\}_h^{[k]} = \sum_{i=1}^{6} C_i^{[k]} \{V\}_i^{[k]} e^{m_i^{[k]}x} \tag{45}$$

The particular solution is obtained as follows

$$\{y\}_p^{[k]} = \left[\left[B_3\right]^{[k]}\right]^{-1} \{F\}^{[k]} \tag{46}$$

Therefore, the total solution for is

$$\{y\}^{[k]} = \sum_{i=1}^{6} C_i^{[k]} \{V\}_i^{[k]} e^{m_i^{[k]} x} + \left[\left[B_3\right]^{[k]}\right]^{-1} \{F\}^{[k]} \tag{47}$$

In general, the problem for each disk consists of 8 unknown values of C_i, namely C_0 (first Eq. (16)), C_1 to C_6 (Eq. (45)), and C_7 (Eq. $u^{[k]} = \int \left(du/dx\right)^{[k]} dx + C_7$).

3.4 Boundary and continuity conditions

According to Fig. 1, the boundary conditions of cone is clamped-clamped ends. Thus, we have

$$\begin{Bmatrix} u \\ \phi \\ w \\ \psi \end{Bmatrix}_{x=0} = \begin{Bmatrix} u \\ \phi \\ w \\ \psi \end{Bmatrix}_{x=L} = \begin{Bmatrix} 0 \\ 0 \\ 0 \\ 0 \end{Bmatrix} \tag{48}$$

Therefore

$$\begin{Bmatrix} U_x\left(x,z\right) \\ U_z\left(x,z\right) \end{Bmatrix}_{x=0,L} = \begin{Bmatrix} 0 \\ 0 \end{Bmatrix} \tag{49}$$

Because of continuity and homogeneity of the cone, at the boundary between two layers, forces, stresses and displacements must be continuous. Given that shear deformation theory applied is an approximation of one order and also all equations related to the stresses include the first derivatives of displacement, the continuity conditions are as follows

$$\begin{Bmatrix} U_x^{[k-1]}\left(x,z\right) \\ U_z^{[k-1]}\left(x,z\right) \end{Bmatrix}_{x=x^{[k-1]}+\frac{t}{2}} = \begin{Bmatrix} U_x^{[k]}\left(x,z\right) \\ U_z^{[k]}\left(x,z\right) \end{Bmatrix}_{x=x^{[k]}-\frac{t}{2}} \tag{50}$$

$$\begin{Bmatrix} U_x^{[k]}\left(x,z\right) \\ U_z^{[k]}\left(x,z\right) \end{Bmatrix}_{x=x^{[k]}+\frac{t}{2}} = \begin{Bmatrix} U_x^{[k+1]}\left(x,z\right) \\ U_z^{[k+1]}\left(x,z\right) \end{Bmatrix}_{x=x^{[k+1]}-\frac{t}{2}} \tag{51}$$

and

$$\begin{Bmatrix} \dfrac{dU_x^{[k-1]}\left(x,z\right)}{dx} \\ \dfrac{dU_z^{[k-1]}\left(x,z\right)}{dx} \end{Bmatrix}_{x=x^{[k-1]}+\frac{t}{2}} = \begin{Bmatrix} \dfrac{dU_x^{[k]}\left(x,z\right)}{dx} \\ \dfrac{dU_z^{[k]}\left(x,z\right)}{dx} \end{Bmatrix}_{x=x^{[k]}-\frac{t}{2}} \tag{52}$$

$$\begin{Bmatrix} \dfrac{dU_x^{[k]}\left(x,z\right)}{dx} \\ \dfrac{dU_z^{[k]}\left(x,z\right)}{dx} \end{Bmatrix}_{x=x^{[k]}+\frac{t}{2}} = \begin{Bmatrix} \dfrac{dU_x^{[k+1]}\left(x,z\right)}{dx} \\ \dfrac{dU_z^{[k+1]}\left(x,z\right)}{dx} \end{Bmatrix}_{x=x^{[k+1]}-\frac{t}{2}} \tag{53}$$

Given the continuity conditions, in terms of Z, 8 equations are obtained. In general, if the cone is divided into n disk layers, $8(n-1)$ equations are obtained. Using the 8 equations of boundary condition, $8n$ equations are obtained. The solution of these equations yields $8n$ unknown constants.

4 RESULTS AND DISCUSSION

The solution described in the preceding section for a homogeneous and isotropic truncated conical shell with $a=40$ mm, $b=30$ mm, $h=20$ mm and $L=400$ mm will be considered. The Young's Modulus, Poisson's ratio, thermal expansion coefficient and thermal conductivity respectively, have values of $E=200Gpa, \nu=0.3, \alpha=12\times10^{-6}1/\,^{\circ}\mathrm{C}$, and $\kappa=20\mathrm{W/m^{\circ}C}$. The internal pressure applied at the $x=0$ and $x=L$ is $P_1=40MPa$ and $P_2=120MPa$ respectively. The truncated cone rotates with $\omega=1000\,rad/s$ and has clamped-clamped boundary conditions. The boundary conditions for temperature are taken as $T_i=100^{\circ}C$ and $T_o=25^{\circ}C$.

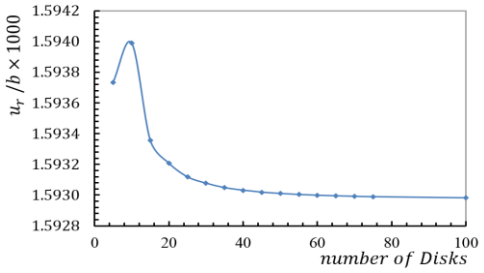

Fig.4
Effect of the number of disk layers on the normalized radial displacement.

The effect of the number of disk layers on the radial displacement is shown in Fig. 4. It could be observed that if the number of disk layers is fewer than 40, it will have a significant effect on the response. However, if the number of layers is more than 60 disks, there will be no significant effect on radial displacement. In the problem in question, 80 disks are used.

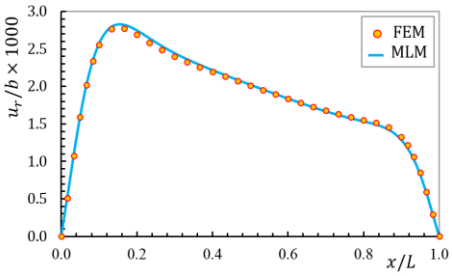

Fig.5
Normalized radial displacement distribution in middle layer.

In Figs. 5-8, displacement and stress distributions are obtained, using MLM, they are then compared with the solutions of FEM and are finally presented in the form of graphs. Figs. 5-8 show that the disk layer method based on FSDT has an acceptable amount of accuracy when one wants to obtain radial displacement, radial stress, circumferential stress and shear stress.

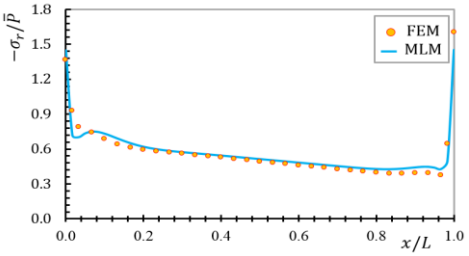

Fig.6
Normalized radial stress distribution in middle layer.

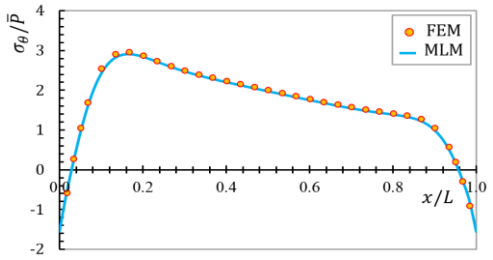

Fig.7
Normalized circumferential stress distribution in middle layer.

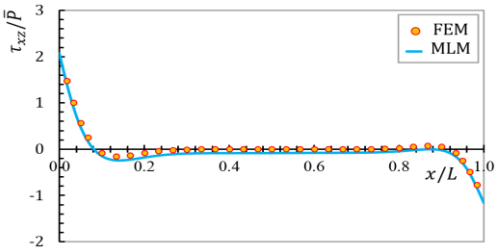

Fig.8
Normalized shear stress distribution in middle layer.

The distribution of normalized radial displacement and stresses across the length of the truncated conical shell subjected to different loading types are shown in Figs. 9-11. As would be expected, it can be seen that the superposition law is satisfied for the thermoelastic analysis of rotating truncated conical shells.

Fig. 9 illustrates the radial displacement distributions change with respect to the internal pressure profile. It can be further observed that the radial displacements subjected to various loading conditions have their peak values some distance away from the boundaries. With regard to Fig. 10, it can be seen that due to edge moments developed, the radial stresses are higher for thermal loading at the clamped ends. Fig. 11 shows that the circumferential stress subjected to centrifugal force and thermal loading at points away from the boundaries at different layers is trivial whereas, at points near the boundaries, the stresses are significant. It must be noted that for the points near the boundaries, the circumferential stress subjected to centrifugal force and internal pressure is more than circumferential stress subjected to total loading whereas for points away from the boundaries, the reverse is the case. The observations above clearly suggest that the centrifugal force is less effective than the internal pressure and thermal loading.

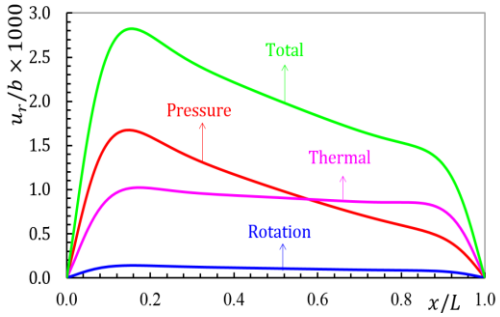

Fig.9
Normalized radial displacement subjected to various loading conditions.

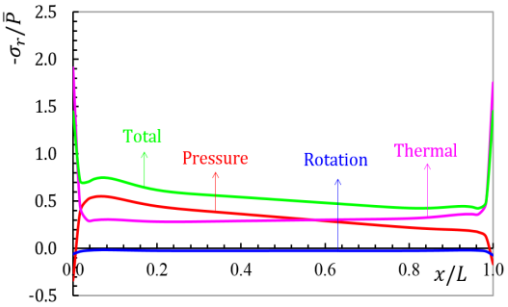

Fig.10
Normalized radial stress subjected to various loading conditions.

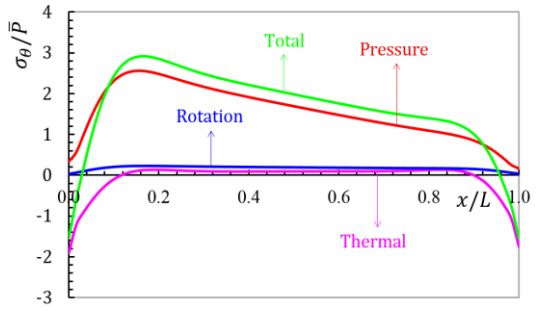

Fig.11
Normalized circumferential stress subjected to various loading conditions.

Fig. 12 shows that a linear pressure distribution can be obtained by setting $m=1$. The pressure profile is concave if $m<1$ and it is convex if $m>1$. Figs. 13 and 14 indicate that radial displacement and circumferential stress rise with increases in non-uniformity pressure constant m. Besides, it could be observed that the radial displacement and circumferential stress distributions change with respect to the internal pressure profile. For example, for convex pressure profile, radial displacement and circumferential stress profile at points away from the boundaries are convex.

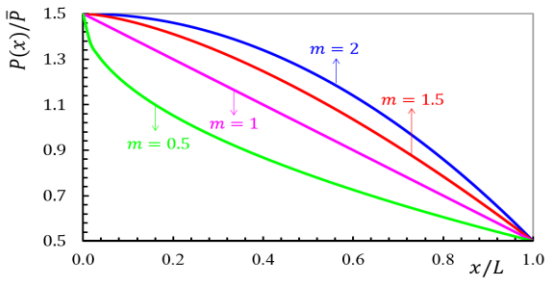

Fig.12
Axial distribution of non-dimensional inner pressure.

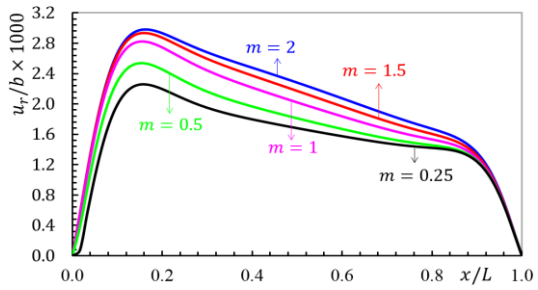

Fig.13
Normalized radial displacement along the length subjected to different internal pressure profiles.

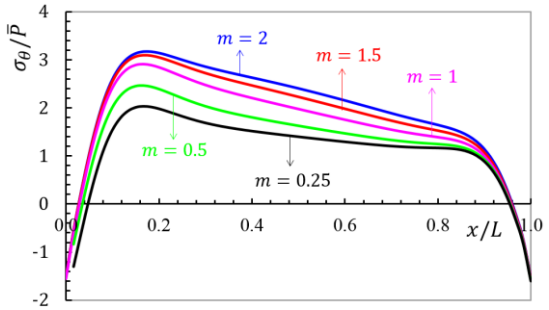

Fig.14
Normalized circumferential stress along the length subjected to different internal pressure profiles.

In order to evaluate the semi-analytical method, a set of results from the FEM were compared with those obtained from the semi- analytical method (Figs. 15-16). The results indicated that the MLM was capable of calculating stress and displacement components in truncated conical shell with great accuracy.

The distribution of radial displacement in the inner surface of the cone is shown in Fig. 15. The greater the tapering angle (i.e., the greater the value of a/b), the greater the radial displacement. The greatest radial

displacement occurs near the lower boundary ($x = 0$). In a like manner, the distribution of the circumferential stress in the inner surface is illustrated in Fig. 16. As this figure suggests, the greater the tapering angle, the greater the circumferential stress.

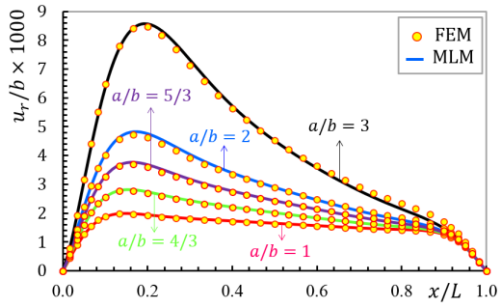

Fig.15
Normalized radial displacement distribution along middle surface with different tapering angles.

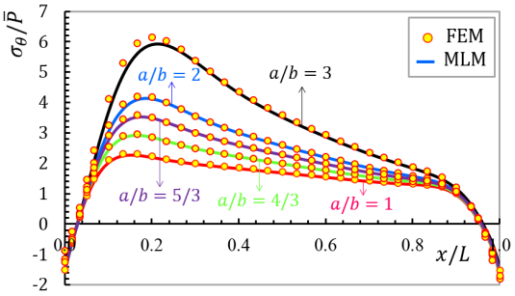

Fig.16
Normalized circumferential stress distribution along middle surface with different tapering angles.

5 CONCLUSIONS

The main objective of the present study was to present an analytical thermoelastic solution for rotating truncated conical shells under non-uniform internal pressure. To this end, based on FSDT and steady state conduction heat transfer equation, the governing equations of thick-walled truncated conical shells were derived. The nonlinear differential equations were derived, using minimum total potential energy principle. A semi-analytical procedure was presented in order to solve the nonlinear differential equations. The thick truncated conical shell was divided into disks with constant height. With regard to the continuity between layers and applying boundary conditions, the governing set of differential equations with constant coefficients was solved. Finite element analysis of the problem, using commercial code was used for the verification purposes of the proposed semi-analytical solution technique. Good agreement was found between the results. From the present study, the following conclusions can be drawn:

- Shear deformation theory (SDT) is a popular model in structural analysis. In SDT, any changes in the axial direction of a thick shell such as geometry parameters and boundary conditions, cause variable coefficients in the governing differential equations. The system of differential equations with variable coefficients can be changed to a set of differential equations with constant coefficients by MLM.
- This approach can be applied to each thick shell with various loadings.
- The results show that the MLM, based on FSDT, has an acceptable amount of accuracy when one wants to obtain radial displacement, radial stress, circumferential stress and shear stress.
- The superposition law is satisfied for the thermoelastic analysis of rotating truncated conical shells.
- The radial displacements subjected to various loading conditions have their peak values some distance away from the boundaries.
- The circumferential stress subjected to centrifugal force and thermal loading at points away from the boundaries at different layers is trivial.
- Case study results show that the centrifugal force is less effective than the internal pressure and thermal loading.
- The thermal circumferential stress is maximum at points near the boundaries.

- The radial displacement and circumferential stress distributions change with respect to the internal pressure profile. For example, for convex pressure profile, radial displacement and circumferential stress profile at points away from the boundaries are convex.
- The radial displacement, and circumferential stress are heavily dependent on tapering angles and any change in the tapering angle brings about a change in them as well.

REFERENCES

[1] Eipakchi H. R., Khadem S. E., Rahimi, G. H., 2008, Axisymmetric stress analysis of a thick conical shell with varying thickness under nonuniform internal pressure, *Journal of Engineering Mechanics* **134**(8): 601-610.

[2] Ghasemi A. R., Kazemian A., Moradi M., 2014, Analytical and numerical investigation of FGM pressure vessel reinforced by laminated composite materials, *Journal of Solid Mechanics* **6**(1): 43-53.

[3] Witt F.J., 1965, Thermal stress analysis of conical shells, *Nuclear Structure Engineering* **1**(5): 449-456.

[4] Panferov I. V., 1991, Stresses in a transversely isotropic conical elastic pipe of constant thickness under a thermal load, *Journal of Applied Mathematics and Mechanics* **56**(3): 410-415.

[5] Jane K. C., Wu Y. H., 2004, A generalized thermoelasticity problem of multilayered conical shells, *International Journal of Solids Structures* **41**: 2205-2233.

[6] Patel B. P., Shukla K. K., Nath Y., 2005, Thermal postbuckling analysis of laminated cross-ply truncated circular conical shells, *Composite Structures* **71**: 101-114.

[7] Vivio F., Vullo V., 2007, Elastic stress analysis of rotating converging conical disks subjected to thermal load and having variable density along the radius, *International Journal of Solids Structures* **44**: 7767-7784.

[8] Naj R., Boroujerdy M. B., Eslami M. R., 2008, Thermal and mechanical instability of functionally graded truncated conical shells, *Thin Walled Structures* **46**: 65-78.

[9] Eipakchi H. R., 2009, Errata for axisymmetric stress analysis of a thick conical shell with varying thickness under nonuniform internal pressure, *Journal of Engineering Mechanics* **135**(9): 1056-1056.

[10] Sladek J., Sladek V., Solek P., Wen P. H., Atluri A. N., 2008, Thermal analysis of reissner-mindlin shallow shells with FGM properties by the MLPG, *CMES: Computer Modelling in Engineering and Sciences* **30**(2): 77-97.

[11] Nejad M. Z., Rahimi G. H., Ghannad M., 2009, Set of field equations for thick shell of revolution made of functionally graded materials in curvilinear coordinate system, *Mechanika* **77**(3): 18-26.

[12] Ghannad M., Nejad M. Z., Rahimi G. H., 2009, Elastic solution of axisymmetric thick truncated conical shells based on first-order shear deformation theory, *Mechanika* **79**(5): 13-20.

[13] Arefi M., Rahimi G. H., 2010, Thermo elastic analysis of a functionally graded cylinder under internal pressure using first order shear deformation theory, *Scientific Research and Essays* **5**(12): 1442-1454.

[14] Jabbari M., Meshkini M., Eslami M. R., 2011, Mechanical and thermal stresses in a FGPM hollow cylinder due to non-axisymmetric loads, *Journal of Solid Mechanics* **3**(1): 19-41.

[15] Ray S., Loukou A., Trimis D., 2012, Evaluation of heat conduction through truncated conical shells, *International Journal of Thermal Sciences* **57**: 183-191.

[16] Ghannad M., Gharooni H., 2012, Displacements and stresses in pressurized thick FGM cylinders with varying properties of power function based on HSDT, *Journal of Solid Mechanics* **4**(3): 237-251.

[17] Ghannad M., Nejad M. Z., Rahimi G. H., Sabouri H., 2012, Elastic analysis of pressurized thick truncated conical shells made of functionally graded materials, *Structural Engineering and Mechanics* **43**(1): 105-126.

[18] Ghannad M., Rahimi G. H., Nejad M. Z., 2013, Elastic analysis of pressurized thick cylindrical shells with variable thickness made of functionally graded materials, *Composite Part B-Engineering* **45**: 388-396.

[19] Nejad M. Z., Jabbari M., Ghannad M., 2014, A semi-analytical solution of thick truncated cones using matched asymptotic method and disk form multilayers, *Archive of Mechanical Engineering* **3**: 495-513.

[20] Nejad M. Z., Rastgoo A., Hadi A., 2014, Effect of exponentially-varying properties on displacements and stresses in pressurized functionally graded thick spherical shells with using iterative technique, *Journal of Solid Mechanics* **6**(4): 366-377.

[21] Nejad M. Z., Jabbari M., Ghannad M. 2014, Elastic analysis of rotating thick truncated conical shells subjected to uniform pressure using disk form multilayers, *ISRN Mechanical Engineering* **764837**: 1-10.

[22] Nejad M. Z., Jabbari M., Ghannad, M., 2015, Elastic analysis of FGM rotating thick truncated conical shells with axially-varying properties under non-uniform pressure loading, *Composite Structures* **122**: 561-569.

[23] Vlachoutsis S., 1992, Shear correction factors for plates and shells, *International Journal for Numerical Methods in Engineering* **33**: 1537-1552.